PNAS RESEARCH ARTICLE | IMMUNOLOGY AND INFLAMMATION

Blockade of the protease ADAM17 ameliorates experimental pancreatitis

Mohamed I. Saad[a,b], Teresa Weng[a,b], Joanne Lundy[a,b,c], Linden J. Gearing[a,b], Alison C. West[a,b], Christopher M. Harpur[a,b], Mohammad Alanazi[a,b], Christopher Hodges[a,b], Daniel Croagh[c], Beena Kumar[d], Irit Sagi[e], Stefan Rose-John[f], and Brendan J. Jenkins[a,b1]

Edited by John O'Shea, NIH, Bethesda, MD; received October 5, 2021; accepted September 9, 2022 by Editorial Board Member Tadatsugu Taniguchi

Acute and chronic pancreatitis, the latter associated with fibrosis, are multifactorial inflammatory disorders and leading causes of gastrointestinal disease-related hospitalization. Despite the global health burden of pancreatitis, currently, there are no effective therapeutic agents. In this regard, the protease A Disintegrin And Metalloproteinase 17 (ADAM17) mediates inflammatory responses through shedding of bioactive inflammatory cytokines and mediators, including tumor necrosis factor α (TNFα) and the soluble interleukin (IL)-6 receptor (sIL-6R), the latter of which drives proinflammatory IL-6 trans-signaling. However, the role of ADAM17 in pancreatitis is unclear. To address this, *Adam17*$^{ex/ex}$ mice—which are homozygous for the hypomorphic *Adam17*^{ex} allele resulting in marked reduction in ADAM17 expression—and their wild-type (WT) littermates were exposed to the cerulein-induced acute pancreatitis model, and acute (1-wk) and chronic (20-wk) pancreatitis models induced by the cigarette smoke carcinogen nicotine-derived nitrosamine ketone (NNK). Our data reveal that ADAM17 expression was up-regulated in pancreatic tissues of animal models of pancreatitis. Moreover, the genetic (*Adam17*$^{ex/ex}$ mice) and therapeutic (ADAM17 prodomain inhibitor [A17pro]) targeting of ADAM17 ameliorated experimental pancreatitis, which was associated with a reduction in the IL-6 trans-signaling/STAT3 axis. This led to reduced inflammatory cell infiltration, including T cells and neutrophils, as well as necrosis and fibrosis in the pancreas. Furthermore, up-regulation of the ADAM17/IL-6 trans-signaling/STAT3 axis was a feature of pancreatitis patients. Collectively, our findings indicate that the ADAM17 protease plays a pivotal role in the pathogenesis of pancreatitis, which could pave the way for devising novel therapeutic options to be deployed against this disease.

ADAM17 | pancreatitis | inflammation | apoptosis | ADAM17 prodomain inhibitor

Significance

Pancreatitis is a multifactorial upper gastrointestinal inflammatory disorder that is associated with substantial morbidity, mortality, and economic burden worldwide. Currently, there are no effective therapeutic agents against either acute or chronic pancreatitis, the latter of which is linked to fibrosis. In this regard, the protease A Disintegrin And Metalloproteinase 17 (ADAM17) mediates inflammatory responses through shedding of bioactive inflammatory mediators, including TNFα and soluble IL-6 receptor (sIL-6R), the latter of which drives proinflammatory IL-6 trans-signaling. However, the role of ADAM17 in pancreatitis is unclear. Here, we define hitherto unknown proinflammatory and profibrotic roles for ADAM17 in promoting pancreatitis possibly via IL-6 trans-signaling. These findings provide a rationale to therapeutically target ADAM17/IL-6 trans-signaling in pancreatitis and other inflammatory conditions.

Pancreatitis is a multifactorial inflammatory disorder and a leading cause for gastrointestinal disease-related hospitalization, which is associated with substantial morbidity, mortality, and economic burden (1, 2). Acute pancreatitis (AP) is a life-threatening condition that is associated with acinar cell necrosis in addition to local and systemic inflammation (3). Globally, 34 people per 100,000 are estimated to develop AP every year, with 20% of those patients developing severe conditions leading to necrosis of the pancreatic tissue and multiple organ failure (3, 4). Moreover, 8% of AP patients develop chronic pancreatitis (CP) (5), which is associated with extensive tissue fibrosis, pancreatic insufficiency, reduced quality of life, and a shorter life expectancy (2). The etiologic causes of AP include gallstones, cigarette smoking, alcohol consumption, hypertriglyceridemia, hypercalcemia, surgery, and trauma, while cigarette smoking and alcohol are the most common risk factors for CP (3, 6). Despite the global burden of the disease, currently, there are no specific and effective therapeutic agents to treat or prevent pancreatitis (2, 5).

The protease A Disintegrin And Metalloproteinase 17 (ADAM17), also known as tumor necrosis factor α (TNFα) converting enzyme (TACE), is a type-I transmembrane protein and a member of the ADAM family of proteases, which consists of 21 members, 13 of which are proteolytically active (7, 8). ADAM17 protein consists of a prodomain, a catalytic domain, a disintegrin domain, a cysteine-rich membrane proximal domain, a single transmembrane domain, and an intracellular cytoplasmic domain (9). The inhibitory prodomain acts as a chaperone for ADAM17, which requires cleavage by furin proteases to release the mature form of ADAM17 (7, 9). Notably, the recombinant prodomain protein (A17pro) has been exploited as a specific inhibitor of ADAM17 cell surface activity in vitro and in vivo, the latter including chronic autoinflammatory and autoimmune disease models (e.g., rheumatoid arthritis and inflammatory bowel disease) (10–12). ADAM17 has emerged as a master regulator of a myriad of physiological and pathological processes, including cell proliferation, immune activation, inflammation, and cancer, owing to its role in ectodomain shedding of a broad spectrum of more than 80 membrane-tethered substrates. These include TNFα, ligands of the epidermal growth

The authors declare no competing interest.

This article is a PNAS Direct Submission. J.O. is a guest editor invited by the Editorial Board.

[1]To whom correspondence may be addressed. Email: brendan.jenkins@hudson.org.au.

This article contains supporting information online at http://www.pnas.org/lookup/suppl/doi:10.1073/pnas.2213744119/-/DCSupplemental.

Published October 10, 2022.

factor receptor (EGFR), Notch receptor, and the interleukin (IL)-6 receptor (IL-6R) (7–9, 13), the latter of which in its soluble form (sIL-6R) drives pathological proinflammatory IL-6 trans-signaling that is associated with pancreatitis severity and lethality (14). Unlike classical IL-6 signaling that controls acute inflammatory responses induced by binding of IL-6 to the membrane-bound IL-6R on target cells, IL-6 trans-signaling requires the formation of a complex between IL-6 and sIL-6R (shed by ADAM17), which then binds to the ubiquitously expressed gp130 coreceptor. Both signaling modes initiate the activation of numerous downstream pathways, namely, Janus kinase/signal transducer and activator of transcription (JAK/STAT), protein kinase B (PKB or AKT), and mitogen-activated protein kinases (MAPKs) including p38 and extracellular signal-regulated protein kinase (ERK1/2) MAPK (15–17). Although ADAM17 has been implicated in the pathogenesis of several inflammatory conditions (7, 13), the role of ADAM17 in pancreatitis remains ill-defined.

In this study, we report that ADAM17 is up-regulated in pancreatic tissues of animal models of pancreatitis. The genetic (using hypomorphic *Adam17*$^{ex/ex}$ mice) and therapeutic (using the ADAM17 prodomain inhibitor, A17pro) targeting of ADAM17 in two independent AP mouse models, cerulein- and cigarette smoke carcinogen (NNK)-induced, ameliorated AP. Furthermore, in an NNK-induced model of CP, *Adam17*$^{ex/ex}$ mice exhibited reduced pancreatic fibrosis. Mechanistically, ADAM17 inhibition significantly suppressed activation of the IL-6 trans-signaling/STAT3 axis, culminating into reduced inflammatory cell infiltration and pancreatic necrosis. Clinically, the ADAM17/IL-6 trans-signaling/STAT3 axis was also up-regulated in pancreatitis patients. Collectively, these data define the proinflammatory role of the protease ADAM17 in promoting pancreatitis and provide a rationale for exploiting ADAM17 inhibitors as therapeutic options for treating or preventing pancreatitis.

Materials and Methods

Human Pancreatic Biopsies. Human pancreatic tissues were collected from patients undergoing surgical resection of a pancreatic mass at Monash Health, Victoria, Australia. Normal pancreatic sections with no histological evidence of neoplasia were obtained by surgical resection for conditions other than pancreatic cancer. Biopsies were fixed in 10% neutral buffered formalin and embedded in paraffin for sectioning and histological analyses. Whole blood was collected from healthy volunteers and pancreatitis patients in EDTA-coated tubes, followed by serum isolation (*SI Appendix*, Table 1). Written and informed patient consent was obtained for each procedure. Studies were approved by the Monash Health Human Research Ethics Committee.

Mice. Age-matched (6- to 8-wk-old) littermates of wild-type (WT) and *Adam17*$^{ex/ex}$ mice, which harbor the hypomorphic *Adam17*^{ex} allele and exhibit significantly reduced global ADAM17 messenger RNA (mRNA) and protein expression (11, 12, 18, 19), were used for experimentation. Mice were housed under specific pathogen-free conditions. Experiments were approved by the Monash University Animal Ethics Committee.

The Cerulein Model of AP. The cerulein-induced mouse model of AP was established via intraperitoneal (IP) injections (1 injection per hour for 7 h) of cerulein (50 μg/kg; Sigma) or phosphate-buffered saline (PBS; 50 μL, as a control). Mice were humanely culled 1 h after the last injection. To assess the efficacy of the therapeutic inhibition of ADAM17 in ameliorating cerulein-induced AP, WT mice were administered a single IP injection of the specific ADAM17 prodomain inhibitor (A17pro; 1 mg/kg), followed by 1 injection per hour for 7 h of cerulein (50 μg/kg). Mice were humanely culled 1 h after the last injection.

The Cigarette Smoke Carcinogen Models of Pancreatitis. For generating the cigarette smoke carcinogen nicotine-derived nitrosamine ketone (NNK)-induced models of pancreatitis, *Adam17*$^{ex/ex}$ were back-crossed with A/J mice for four generations to produce mice on a pseudo-A/J background, which are susceptible to the cytotoxic effects of NNK (12, 20). WT and *Adam17*$^{ex/ex}$ mice received three IP injections on alternate days over a week of either NNK (100 mg/kg; Toronto Research Chemicals) dissolved in PBS or equivalent volume of PBS as a control (12). Mice were humanely culled the following week (acute setting) or 20 wk after NNK challenge (chronic setting). To evaluate the therapeutic potential of the ADAM17 prodomain in ameliorating NNK-induced AP, WT mice were administered three IP injections of the ADAM17 prodomain (A17pro; 1 mg/kg) on alternate days simultaneously with NNK (100 mg/kg) over a week.

Sera and pancreatic tissues were collected at the end of the experiments, and pancreatic tissues were either formalin-fixed and paraffin-embedded (FFPE) or snap-frozen in liquid nitrogen and stored at −80 °C for further molecular analyses.

Primary Murine Acinar Cell Cultures and Cocultures. Primary murine pancreatic acini from WT and *Adam17*$^{ex/ex}$ mice were isolated and maintained in culture as described previously (21). Briefly, pancreatic tissues were dissected, then enzymatically and mechanically dissociated in a digestion solution containing Hank's Balanced Salt Solution (HBSS; Sigma), HEPES (10 mM; Sigma), collagenase IA (200 U/mL; Sigma), and trypsin inhibitor (0.25 mg/mL; Sigma) at 37 °C. The enzymatic digestion then stopped using cold washing solution containing HBSS, 5% Fetal Bovine Serum (FBS; Sigma), and HEPES (10 mM), prior to resuspending acini cells in Waymouth's medium (Sigma) containing 2.5% FBS, trypsin inhibitor (0.25 mg/mL), 1% penicillin/streptomycin (Sigma), and recombinant human epidermal growth factor (EGF; 25 ng/mL; Lonza). Cells were then cultured in six-well plates for 24 h at 37 °C under 5% CO_2 conditions. Thereafter, the nonadherent acini were transferred into a coated 24-well plate with type I collagen (Sigma) for 2 d at 37 °C under 5% CO_2 to facilitate acini adherence. Acinar cell cultures were treated with cerulein (10 μM), NNK (1 μM), or PBS (as a control), for 24 h before supernatants and cells were collected for subsequent analyses.

For acinar and T cell coculture experiments, T cells were isolated from spleens of WT or *Adam17*$^{ex/ex}$ mice (subjected to 1 injection per hour for 7 h of cerulein to induce pancreatitis) using EasySep Mouse T Cell Isolation Kit (STEMCELL Technologies) according to the manufacturer's instructions. Isolated T cells were then added to adherent acinar cell cultures at a ratio of 1:1, and the coculture was subjected to cerulein stimulation (10 μM) for 24 h before cells and supernatants were collected for subsequent analyses.

Expression and Purification of ADAM17 Prodomain Inhibitor (A17pro). The generation of A17pro has been previously reported (10). Briefly, electrocompetent *Escherichia coli* BL21 (DE3) were transformed with the corresponding ADAM17 prodomain sequence in pET28 plasmid, following which sonicated bacterial supernatants were applied to a Ni^{+2} column (GE Healthcare) and eluted with buffer containing 50 mM Tris, 300 mM NaCl, and 250 mM imidazole. The eluted protein was dialyzed and applied to a HiTrap Q HP column (GE Healthcare). The fraction containing A17pro protein was subjected to size exclusion chromatography using Superdex 75 (GE Healthcare). Using fresh tissue imaging analysis, purified recombinant A17pro could be detected 10 h following injection in vivo (10).

RNA Isolation, Gene Expression Analyses, and RNA Transcriptome Sequencing. Total RNA was isolated from snap-frozen mouse pancreatic tissues or acini cultures using TRIzol (Sigma), and quantitative RT-PCR (qPCR) was performed on cDNA with Power SYBR (Life Technologies) using the QuantStudio 6 Flex Real-Time PCR System (Applied Biosystems). Gene expression data acquisition and analyses were performed using the QuantStudio 6 Flex Real-Time PCR System Software (Applied Biosystems). Primer sequences are available in *SI Appendix*, Table S2.

RNA transcriptome sequencing (RNA-Seq) was performed by the Monash Health Translational Precinct Medical Genomics Facility. Briefly, total RNA concentration was quantified by Qubit (Invitrogen) and quality checked by Bioanalyzer (Agilent). Libraries were generated using an in-house multiplex RNA-Seq method and were prepared using 30 ng of total RNA input. An 8-bp sample index and a 10-bp unique molecular identifier (UMI) were added during initial poly(A) priming, and pooled samples were amplified using a template switching oligonucleotide. Illumina P5 was added by tagmentation via Nextera transposase and PCR, and Illumina P7 was added by PCR. The library was designed so that the forward read (R1) used the standard R1 primer to sequence the cDNA in the

sense direction for transcript identification. The index read (I1) used the standard I7 primer to sequence directly into the sample index and then the 10-bp UMI. Sequencing was performed on an Illumina NextSeq 2000 using a P2 100 cycle kit, as per the manufacturer's instructions (Life Technologies). Onboard denaturing and clustering were done using 1,000 pM of library pool (Illumina Protocol 1000000109376 v3, November 2020). Base calling was performed using Dragen BCLConvert (v3.7.4).

RNA-Seq read alignment and UMI counting was performed in R (v4.1.2) (22). The scPipe package (v1.16.0) (23) was employed to process the data. Read alignment was performed using the RSubread package (v2.8.1) (24). An index was built using the Ensembl Mus musculus GRCm38 primary assembly genome file, and alignment was performed with default settings. Aligned reads were mapped to exons using the sc_exon_mapping function with the Ensembl Mus musculus GRCm38 v100 GFF3 genome annotation file. Additional gene annotation was obtained using the biomaRt package (v2.50.1) (25), and a DGEList object was created with the counts and gene annotation using the edgeR package (v3.36.0) (26). A design matrix was constructed incorporating the experimental group, combining genotype and treatment. Lowly expressed genes were removed using the filterByExpr function, and normalization factors were calculated using the default method (27). Counts were transformed using the voom method (28), and a linear model was fit using the edgeR voomLmFit function. Differential gene expression analyses were performed using the limma (v3.50.0) package (29). Groups were compared using the contrasts.fit function, and moderated *t* statistics were calculated relative to a 1.2-fold threshold using the treat function (30). Differentially expressed genes were determined using a false discovery rate (FDR)-adjusted $P < 0.05$. Heat maps were created using the pheatmap package (v1.0.12) (31). Log_2 counts per million (CPM) expression values were calculated using the edgeR cpm function. Relative Log_2 CPM expression values were calculated for each gene by subtracting the average Log_2 CPM value of WT controls. Heat map scales were truncated at ±5. Gene set collections were obtained from the Broad Institute Molecular Signature Database (32) via the msigdbr package (v7.4.1) (33). Gene set testing was performed using the cameraPR function (34) from the limma package on moderated *t* statistics obtained without a fold-change threshold using the eBayes function (35). The union of the top 10 most significant gene sets from WT mice (cerulein versus PBS) and the top 10 most significant gene sets from *Adam17*$^{ex/ex}$ mice (cerulein versus PBS) were selected, and the results were displayed as bar plots.

Immunohistochemistry. FFPE human pancreatic sections were stained with antibodies against ADAM17 (Sigma) and pTyr^{705}-STAT3 (Cell Signaling Technology). Mouse pancreatic FFPE sections were subjected to immunohistochemistry (IHC) with the following antibodies: ADAM17, α-Smooth muscle actin (αSMA; Sigma), CD45, B220 (BD Biosciences), CD11c, cleaved caspase-3, pThr^{180}/pTyr^{182}-p38 MAPK, pThr^{202}/pTyr^{204}-ERK1/2 MAPK, pTyr^{705}-STAT3, pSer^{536} p65 nuclear factor-κB (NF-κB), pSer^{473} AKT (Cell Signaling Technology), CD3, Ly6G, and F4/80 (Abcam). Cellular apoptosis was determined by the terminal deoxynucleotidyl transferase (tdT)-mediated dUDP nick-end labeling (TUNEL) technique using the ApopTag Peroxidase In Situ Apoptosis Detection kit (Millipore). Masson's trichome staining was performed using standard protocols at Monash Histology Platform. To quantify cellular staining, digital images of photomicrographs (60× high-power fields) were viewed using Image J software. Positive-stained cells were counted manually or staining intensity was quantified using Image J software ($n = 20$ fields).

Immunofluorescence. Mouse FFPE pancreatic sections were subjected to immunofluorescence evaluation by staining with antibodies against ADAM17 (Sigma), CD45 (BD Biosciences), IL-6R (Santa Cruz Biotechnology), E-cadherin, and Vimentin (Cell Signaling Technology). Alexa Fluor conjugates (Invitrogen) were used as secondary antibodies. Nuclear staining was achieved using 4,6-diamidino-2-phenylindole (DAPI). Negative controls in the absence of primary antibodies were performed to indicate the level of background autofluorescence.

Enzyme-Linked Immunosorbent Assay. IL-6R levels were measured in human sera, as well as mouse sera and acinar cell culture supernatants, using human and mouse IL-6R enzyme-linked immunosorbent assay (ELISA) sets from R&D Systems, respectively. Mouse serum IL-6 levels were measured using mouse IL-6 ELISA sets from R&D Systems.

Amylase and Lipase Assays. Serum levels of mouse amylase and lipase enzymes were determined using amylase and lipase colorimetric assay kits, respectively, from Abcam.

Statistical Analyses. All statistical analyses were performed using GraphPad Prism, version 8.0. Where appropriate, Student's *t* test or one-way ANOVA were used to determine differences between groups. $P < 0.05$ was considered statistically significant. Data are expressed as the mean ± SEM.

Results

ADAM17 Expression Is Up-Regulated in Cerulein-Induced AP. First, we sought to investigate the expression of ADAM17 in pancreatic tissues of WT mice treated with either PBS or cerulein. ADAM17 mRNA and protein levels were significantly up-regulated by 5- and 2.2-fold, respectively, in cerulein-treated pancreata compared to their controls (Fig. 1 *A*–*C*). ADAM17 mRNA expression was also significantly enhanced in mouse pancreatic acinar cell cultures upon stimulation with cerulein in vitro (Fig. 1*D*). Consistent with a previous report showing that ADAM17 is expressed in different pancreatic compartments (36), ADAM17 staining was widely distributed in the E-cadherin–positive epithelial pancreatic compartment consisting of acinar cells (Fig. 1*E*), the major site of pancreatitis onset (37). ADAM17 was also detected in CD45-positive pan-immune cell infiltrates, and to a minimal extent in the vimentin-positive endothelial compartment, in cerulein-treated pancreatic tissues (Fig. 1*E*). These findings suggest that the ADAM17 protease may play a crucial role in the pathogenesis of pancreatitis.

ADAM17 Deficiency Ameliorates Cerulein-Induced AP. To assess the role of ADAM17 in promoting pancreatitis, we employed *Adam17*$^{ex/ex}$ mice, which are homozygous for the hypomorphic *Adam17*^{ex} allele resulting in reduced global ADAM17 expression including in pancreatic tissues and the epithelial acinar cell compartment (*SI Appendix*, Fig. 1 *A* and *B*). The *Adam17*$^{ex/ex}$ mice and their WT littermates received 1 injection per hour for 7 h of either PBS (as a control) or supramaximal doses of cerulein. Histopathological scoring of pancreatic tissues showed that the pancreatitis phenotype was markedly ameliorated in *Adam17*$^{ex/ex}$ mice compared to their WT counterparts, as indicated by lower immune cell infiltration, necrotic acinar cells, and edema (Fig. 1 *F* and *G*). Furthermore, serum levels of amylase were significantly higher in cerulein-treated WT mice compared to *Adam17*$^{ex/ex}$ mice, with levels in the latter comparable to WT and *Adam17*$^{ex/ex}$ mice treated with PBS (Fig. 1*H*). These data indicate that ADAM17 promotes pancreatic inflammation and acinar cell necrosis in the cerulein-induced model of AP.

ADAM17 Induces Immune Cell Infiltration and Acinar Cell Death in AP. To determine the composition of the immune cell infiltration in pancreatic tissues, we employed IHC on pancreas sections from WT and *Adam17*$^{ex/ex}$ mice treated with cerulein versus PBS. Numbers of CD45-positive immune/inflammatory cells were significantly increased in pancreatic tissues of WT mice treated with cerulein compared to their *Adam17*$^{ex/ex}$ counterparts (Fig. 2 *A* and *B*). The majority of these immune infiltrations were identified as CD3-positive T cells, which were also significantly reduced in cerulein-treated *Adam17*$^{ex/ex}$ mice compared to their WT controls (Fig. 2 *C* and *D*). In contrast, minimal numbers of Ly6G-postive neutrophils, F4/80-positive macrophages, B220-positive B cells, CD11c-positive dendritic cells, and mast cells were detected in pancreatic tissues, with numbers of Ly6G-positive neutrophils significantly lower in cerulein-treated *Adam17*$^{ex/ex}$ mice (*SI Appendix*, Fig. 2 *A*–*J*). Consistently, mRNA levels of inflammatory chemokines that

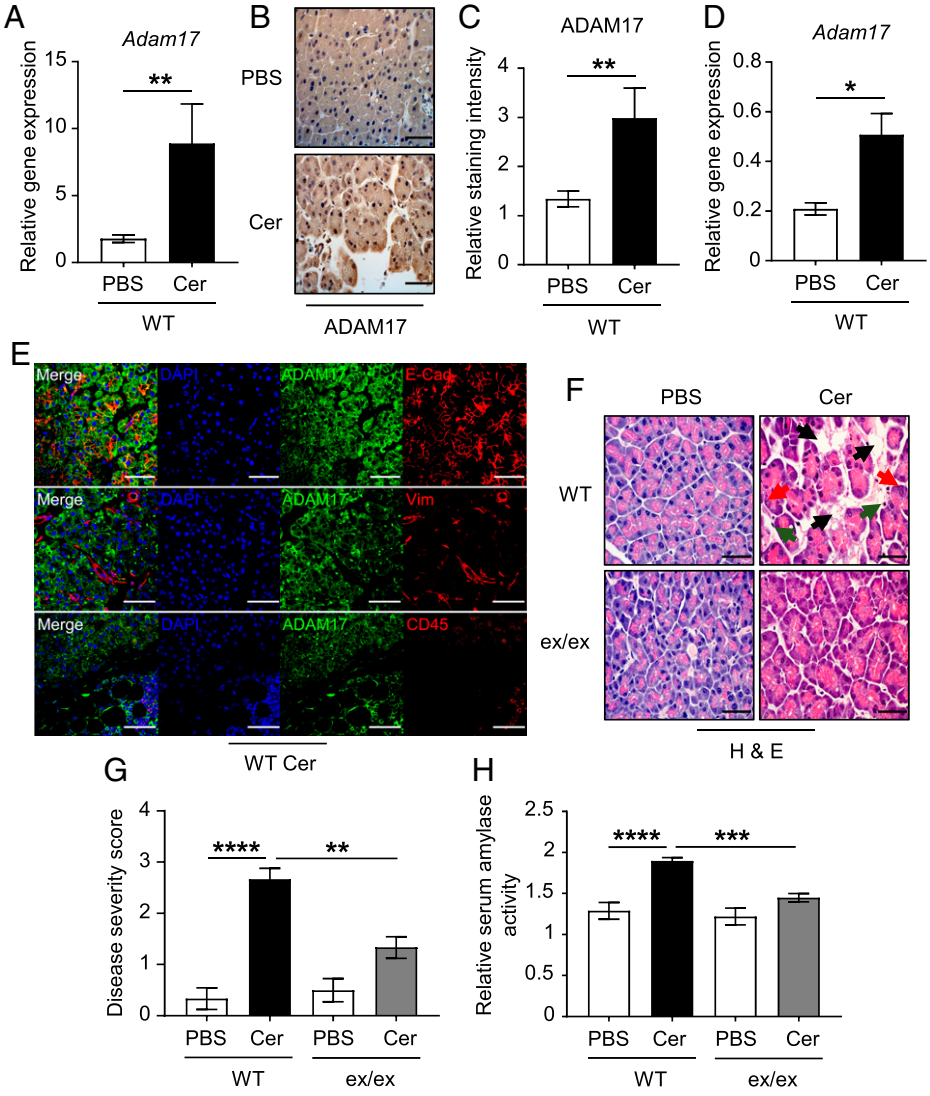

Fig. 1. ADAM17 deficiency ameliorates cerulein-induced AP. (*A*) qPCR expression analysis of *Adam17* gene (normalized against *18s rRNA*) in pancreatic tissues from WT mice treated with either PBS (as a control) or cerulein (Cer) (n = 5 per group). **P < 0.01, Student's t test. (*B*) Representative images of ADAM17-stained pancreatic sections from PBS or cerulein-treated WT mice. (Scale bar, 100 μm) (*C*) Quantification of ADAM17 staining intensity in pancreatic tissues of the indicated groups (n = 5 per group). **P < 0.01, Student's t test. (*D*) qPCR expression analysis of the *Adam17* gene (normalized against *18s rRNA*) in pancreatic acinar cell cultures from WT mice treated with either PBS or cerulein (Cer) (n = 3 to 5 per group). *P < 0.05, Student's t test. (*E*) Representative immunofluorescence images of pancreatic sections from cerulein-treated mice costained for ADAM17 and markers for epithelial cells (E-cadherin [E-Cad]), endothelial cells (Vimentin [Vim]), and total immune cells (CD45). DAPI nuclear staining is blue. (Scale bars, 100 μm) (*F*) Representative images of H&E-stained pancreatic sections from WT mice and *Adam17*$^{ex/ex}$ mice (ex/ex) treated with either PBS or cerulein (Cer). Black arrowheads point to edematous areas, green arrowheads point to immune cell infiltration, and red arrowheads point to necrotic cells. (Scale bars, 100 μm) (*G*) Histological disease severity scoring of pancreatic edema, necrosis, and inflammation in pancreatic tissues from the indicated groups (n = 6 to 8 per group). (*H*) Relative serum amylase activity in the indicated groups (n = 6 to 8 per group). **P < 0.01, ***P < 0.001, ****P < 0.0001, one-way ANOVA.

are implicated in the pathogenesis of pancreatitis, as well as modulating immune cell function (14, 38–41), were significantly reduced in pancreatic tissues of cerulein-treated *Adam17*$^{ex/ex}$ mice compared to their WT littermates (Fig. 2*E*).

Acinar cell death is a hallmark of cerulein-induced pancreatitis (42). Therefore, we assessed acinar cell injury using IHC-based TUNEL and cleaved caspase-3 assays. ADAM17 deficiency in the *Adam17*$^{ex/ex}$ mice significantly ameliorated acinar cell injury as indicated by 52 and 43% reduction in TUNEL and cleaved caspase-3 staining, respectively, compared to their WT counterparts (Fig. 2 *F* and *G* and *SI Appendix*, Fig. 2 *K* and *L*). Collectively, these findings implicate the ADAM17 protease as a critical mediator in the pathogenesis of pancreatic inflammation and acinar cell injury.

ADAM17 Promotes AP, Which Is Associated with Elevated IL-6 Trans-signaling Pathways. Next, we sought to delineate the mechanistic basis of the ADAM17-promoting role in AP. Supraphysiological doses of cerulein are a well-known inducer of a wide range of genes involved in tissue inflammation and injury, including IL-6, IL-1β, and TNFα via activation of the transcription factor NF-κB (43). While levels of phosphorylated/activated p65 NF-κB were significantly induced in cerulein-treated pancreatic tissues of WT mice, they were significantly lower in their *Adam17*$^{ex/ex}$ counterparts (Fig. 3 *A* and *B*). Also, elevated pancreatic mRNA and serum protein levels of IL-6 in cerulein-treated WT mice were significantly reduced in cerulein-treated *Adam17*$^{ex/ex}$ mice (Fig. 3 *C* and *D*). Moreover, the genetic deficiency of ADAM17 in *Adam17*$^{ex/ex}$ mice markedly reduced serum levels of sIL-6R, the master regulator of the pathological IL-6 trans-signaling (8, 14, 17) (Fig. 3*E*). Interestingly, immunofluorescence analysis revealed that the ubiquitously expressed ADAM17 in the acinar cell compartment of cerulein-treated WT mice is highly colocalized with the IL-6R, suggesting unrestricted ADAM17 accessibility to its substrate (Fig. 3*F*). Moreover, ADAM17-deficient acinar cell cultures exhibited significant reduction in *Il6* mRNA levels and IL-6R shedding capabilities following treatment with cerulein, compared to their WT controls (Fig. 3 *G* and *H*).

Consistent with suppressed levels of IL-6 and sIL-6R in cerulein-treated *Adam17*$^{ex/ex}$ pancreas samples, activation (phosphorylation) of STAT3 signaling, which is a major pathway employed by IL-6 trans-signaling, was decreased in cerulein-treated *Adam17*$^{ex/ex}$ mice compared to their WT controls, as was expression of the STAT3-target gene, *Socs3* (Fig. 3 *I–K*). Moreover, activated levels of ERK1/2 and p38 MAPKs, which are implicated in the pathogenesis of the cerulein-induced AP (44–47), were significantly reduced in pancreatic tissues of the cerulein-treated *Adam17*$^{ex/ex}$ mice compared to their WT controls (*SI Appendix*, Fig. 3 *A–D*), whereas levels of

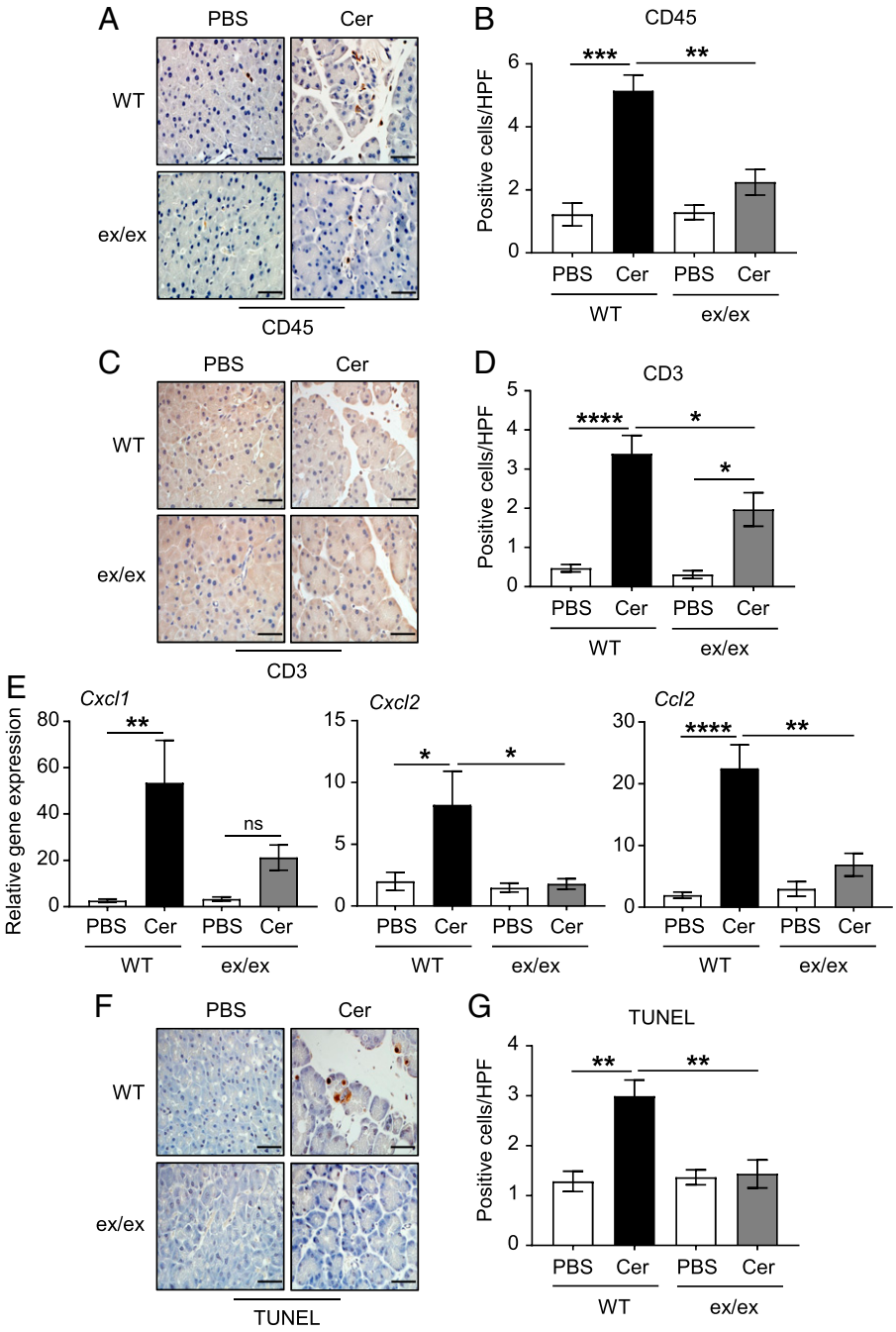

Fig. 2. ADAM17 promotes pancreatic immune cell infiltration, inflammation and acinar cell death in the cerulein-induced AP model. (*A, C,* and *F*) Representative images of CD45, CD3, and TUNEL-stained pancreatic sections from WT mice and *Adam17*$^{ex/ex}$ mice (ex/ex) treated with either PBS or cerulein (Cer), respectively. (Scale bars, 100 μm) (*B, D,* and *G*) Quantification of CD45, CD3, and TUNEL-positive cells per high-power field (HPF) in pancreatic tissues of the indicated groups, respectively ($n = 6$ to 8 per group). (*E*) qPCR expression analysis of inflammatory genes (normalized against *18s rRNA*) in pancreatic tissues from the indicated mice ($n = 5$ to 7 per group). *$P < 0.05$, **$P < 0.01$, ***$P < 0.001$, ****$P < 0.0001$; ns, not significant, one-way ANOVA.

activated AKT were unchanged (*SI Appendix*, Fig. 3 *E* and *F*). Taken together, these data suggest that ADAM17 employs IL-6 trans-signaling via multiple pathways (e.g., STAT3) to promote AP.

Transcriptomics Analysis of ADAM17-Dependent Molecular Pathways Implicated in AP. To further understand the molecular basis by which ADAM17 promotes AP, we employed RNA-Seq to profile the differential regulation of gene networks in pancreatic tissues of WT and *Adam17*$^{ex/ex}$ mice subjected to cerulein-induced AP (compared to their PBS controls). Differential expression analysis clearly distinguished the pancreatic gene expression profile of cerulein-treated WT mice from their PBS counterparts, with 1,247 and 1,320 genes significantly up-regulated and down-regulated, respectively, in pancreatic tissues. These differences in gene expression were markedly reduced in pancreatic tissues of cerulein-treated *Adam17*$^{ex/ex}$ mice compared to their PBS controls (Fig. 4*A*). To identify enriched ADAM17-regulated gene networks aligned to molecular functions and biological processes in pancreatitis, we next performed competitive gene set testing on gene expression data of pancreatic tissues from WT or *Adam17*$^{ex/ex}$ mice (cerulein-treated versus PBS-treated). Our analysis identified multiple cytokine signaling pathways, including IL-6 signaling via activation of JAK/STAT3, which were significantly up-regulated in pancreatic tissues of WT mice treated with cerulein compared to their PBS controls (Fig. 4*B*). Notably, among these pathways, IL-6/JAK/STAT3 signaling was reduced in pancreatic tissues of *Adam17*$^{ex/ex}$ mice treated with cerulein compared to their WT counterparts (adjusted $P = 0.08$). Furthermore, our RNA-Seq data identified clusters of genes that were significantly up-regulated in pancreatic tissues of cerulein-treated WT versus *Adam17*$^{ex/ex}$ mice (Fig. 4*C*), several of which have been implicated in the pathogenesis of

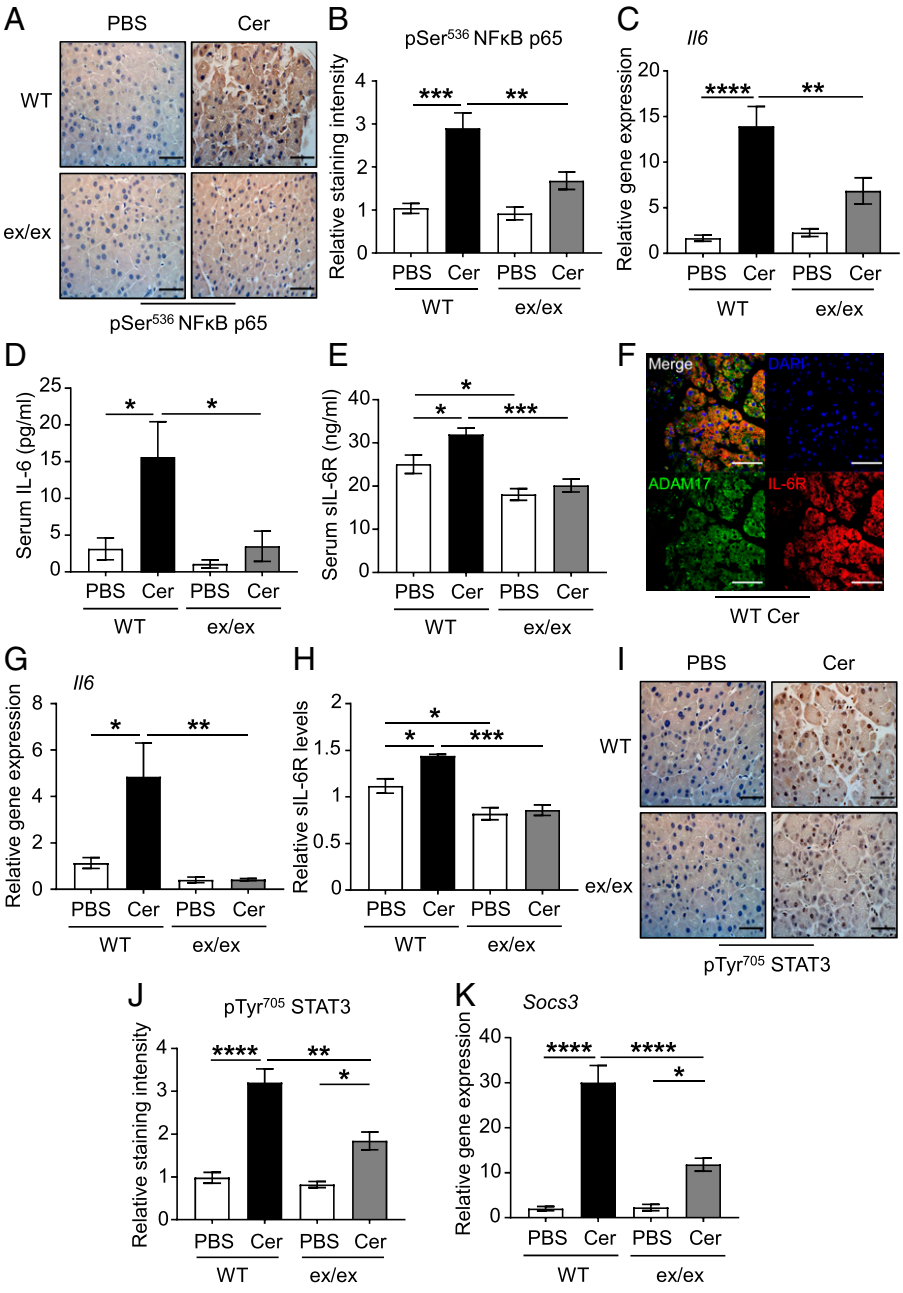

Fig. 3. Genetic targeting of ADAM17 diminishes the expression of the components of the pathological IL-6 trans-signaling. (*A*) Representative images of pSer^{536} p65 NFκB-stained pancreatic sections from WT mice and *Adam17*$^{ex/ex}$ mice (ex/ex) treated with either PBS (as a control) or cerulein (Cer). (Scale bars, 100 μm) (*B*) Quantification of pSer^{536} p65 NFκB-staining intensity in pancreatic tissues of the indicated groups (n = 5 per group). (*C*) qPCR expression analysis of *Il6* gene (normalized against *18s rRNA*) in pancreatic tissues from the indicated mice (n = 5 to 7 per group). (*D* and *E*) Serum levels of IL-6 (pg/mL) and soluble IL-6R (sIL-6R; ng/mL) in the indicated groups (n = 5 to 7 per group). (*F*) Representative immunofluorescence images of pancreatic sections from cerulein-treated mice co-stained for ADAM17 and IL-6R. DAPI nuclear staining is blue. (Scale bars, 100 μm) (*G*) qPCR expression analysis of *Il6* gene (normalized against *18SrRNA*) in pancreatic acinar cell cultures from WT and *Adam17* $^{ex/ex}$ mice treated with either PBS or cerulein (Cer) (n = 3 to 5 per group). (*H*) Relative soluble IL-6R levels (sIL-6R) in pancreatic acinar cell culture supernatants from the indicated groups (n = 3 to 5 per group). (*I*) Representative images of pTyr^{705} STAT3-stained pancreatic sections from WT and *Adam17*$^{ex/ex}$ mice treated with either PBS or cerulein (Cer). (Scale bars, 100 μm) (*J*) Quantification of pTyr^{705} STAT3-staining intensity in pancreatic tissues of the indicated groups (n = 5 per group). (*K*) qPCR expression analysis of *Socs3* gene (normalized against *18s rRNA*) in pancreatic tissues from the indicated mice (n = 5 to 7 per group). *P < 0.05, **P < 0.01, ***P < 0.001, ****P < 0.0001, one-way ANOVA.

pancreatitis and/or pancreatic cancer, including *Krt8*, *Krt18*, *Krt19*, *Hmga1*, and *Clic1* (48–52).

ADAM17-Expressing Epithelial Cells Play a Major Role in Driving Pathological IL-6 Trans-signaling In Vitro. Since ADAM17 is detected in both epithelial and immune cell compartments within the pancreas (Fig. 1*E*), with the majority of immune cell infiltrates being T cells (Fig. 2*D*), we sought to investigate the relative contribution of ADAM17 in both compartments in driving IL-6 trans-signaling. Therefore, we established reciprocal primary murine acinar and T cell cocultures from WT and *Adam17*$^{ex/ex}$ mice, which were stimulated with cerulein in vitro. Our data reveal that *Adam17* mRNA levels were significantly reduced only in cultures comprising *Adam17*$^{ex/ex}$ acinar cells (i.e., irrespective of the presence of either WT and *Adam17*$^{ex/ex}$ T cells), which suggests that the up-regulation of ADAM17 gene expression in response to cerulein treatment is mainly due to ADAM17 overexpression in the epithelial compartment (Fig. 4*D*). Consistent with our in vivo data, we also observed that sIL-6R shedding levels, as well as expression levels of *Il6* and *Socs3*, were significantly down-regulated when ADAM17 is abolished in the epithelial compartment (i.e., in *Adam17*$^{ex/ex}$ acinar cells), again irrespective of the genotype of cocultured T cells (Fig. 4 *E*–*G*). Therefore, these data suggest that ADAM17 expression in acinar epithelial cells plays a major role in mediating signaling cascades downstream of ADAM17 during pancreatitis, with a lesser contribution of T cells to ADAM17-driven signaling pathways in pancreatitis.

ADAM17 Deficiency Ameliorates Cigarette Smoke Carcinogen-Induced Pancreatic Inflammation. Having established the requirement of ADAM17 for promoting cerulein-induced AP, we next validated this requirement in an independent model of AP induced by the cigarette smoke carcinogen (NNK). For this purpose, WT and *Adam17*$^{ex/ex}$ were bred on the pseudo-A/J background, which is susceptible for the toxic effects of NNK

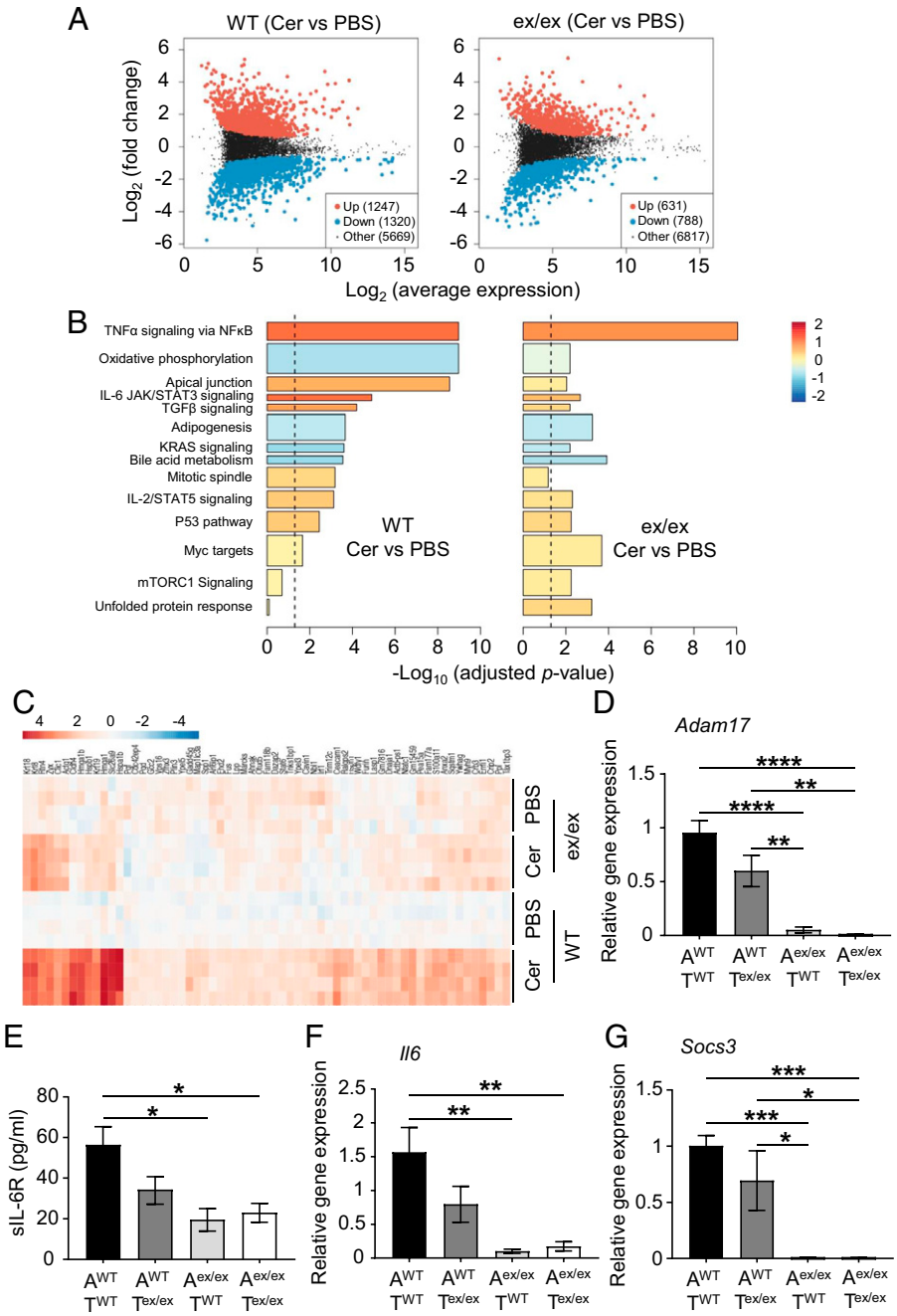

Fig. 4. RNA-Seq analysis of ADAM17-dependent molecular pathways implicated in AP in vivo and analysis of IL-6 trans-signaling components in ADAM17-expressing epithelial versus T cells in vitro. (*A*) Plots showing the Log_2 (average gene expression) and Log_2 (fold change) between pancreatic tissues of WT or *Adam17*$^{ex/ex}$ (ex/ex) mice treated with either PBS (as a control) or cerulein (Cer), with significantly differentially up- and down-regulated genes highlighted in red and blue, respectively ($P < 0.05$). (*B*) Bar plots of camera gene set tests showing some of the most significantly enriched gene sets from the MSigDB Hallmark gene set collection in pancreatic tissues of WT mice (Cer versus PBS) and *Adam17*$^{ex/ex}$ mice (Cer versus PBS), ordered by significance in WT samples. Bar length represents $-Log_{10}$ (adjusted *P* value), color indicates mean Log_2 (fold change) of all genes in the gene set, and bar width reflects the relative gene set size. The dashed line shows FDR (adjusted *P* value) = 0.05. (*C*) Heat map showing the relative Log_2 expression of genes induced in pancreatic tissues of WT mice treated with cerulein compared to their PBS controls, for which induction was significantly higher in WT mice (Cer versus PBS) than in *Adam17*$^{ex/ex}$ mice (Cer versus PBS). Gene expression in all samples is relative to the average of the PBS-treated WT controls. (*D*) qPCR expression analysis of *Adam17* gene (normalized against *18s rRNA*) in acinar (A) and T cell (T) cocultures from WT or *Adam17*$^{ex/ex}$ mice treated with cerulein ($n = 3$ to 4 per group). (*E*) Soluble IL-6R (sIL-6R; pg/mL) in supernatants of the indicated cocultures ($n = 3$ to 4 per group). (*F* and *G*) qPCR expression analysis of *Il6* and *Socs3* genes (normalized against *18s rRNA*) in the indicated cocultures, respectively ($n = 3$ to 4 per group). $^*P < 0.05$, $^{**}P < 0.01$, $^{***}P < 0.001$, $^{****}P < 0.0001$, one-way ANOVA.

(12, 20, 53). Consistent with the cerulein AP model, ADAM17 mRNA and protein levels were up-regulated in the NNK-treated WT mice compared to their PBS-treated controls (Fig. 5*A* and *SI Appendix*, Fig. 4 *A* and *B*). Also, ADAM17 mRNA expression was elevated in NNK-treated acinar cells in vitro (*SI Appendix*, Fig. 4*C*). In addition, ADAM17 was predominantly expressed in the E-cadherin epithelial compartment of pancreatic tissues following NNK challenge (*SI Appendix*, Fig. 4*D*).

Histopathological assessment of pancreatic tissues from PBS-treated WT, as well as NNK-treated WT and *Adam17*$^{ex/ex}$ mice, revealed that ADAM17 deficiency in *Adam17*$^{ex/ex}$ mice protected against disease severity, as indicated by reduced edema and inflammatory infiltration (Fig. 5 *B* and *C*). Unlike the cerulein model, challenging mice with NNK did not induce acinar cell death (Fig. 5*B*). Since this model is generated over 10 d, serum lipase activity was used as a biomarker for AP, which offers a larger diagnostic window than amylase (i.e., its levels increase over a longer time) (54). Serum lipase levels were also significantly elevated in NNK-treated WT mice compared to their PBS controls and *Adam17*$^{ex/ex}$ littermates (Fig. 5*D*). Consistent with the ameliorated pancreatitis phenotype seen in *Adam17*$^{ex/ex}$ mice, numbers of CD45-positive immune cells infiltrating the pancreas were markedly reduced, including CD3 T cells (Fig. 5 *E* and *F* and *SI Appendix*, Fig. 4 *E* and *F*). Genetic targeting of ADAM17 also suppressed NNK-induced activation of NF-κB, generation of IL-6 as well as ectodomain shedding of sIL-6R, including from acinar epithelial cells, and activation of STAT3 in pancreatic tissues (Fig. 5 *G–L* and *SI Appendix*, Fig. 4 *G–I*). In contrast, levels of cleaved caspase-3, as well as activated MAPKs and AKT, were unchanged in NNK-treated *Adam17*$^{ex/ex}$ mice compared to their WT littermates (*SI Appendix*, Fig. 5 *A–H*). These findings indicate that ADAM17 is a crucial driver of IL-6 trans-signaling-induced

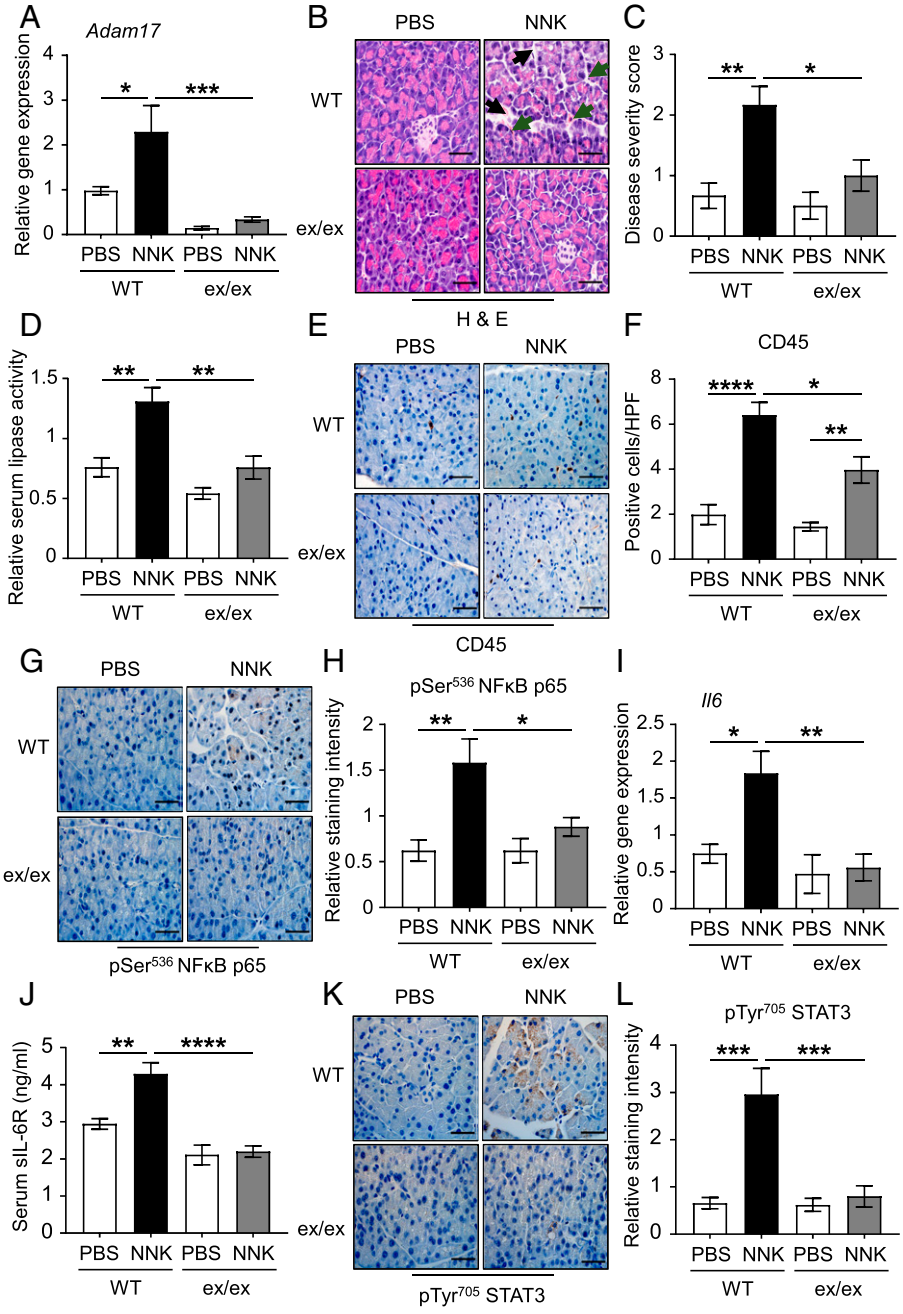

Fig. 5. ADAM17 promotes cigarette smoke carcinogen (NNK)-induced pancreatic inflammation. (*A*) qPCR expression analysis of *Adam17* gene (normalized against *18S rRNA*) in pancreatic tissues from PBS (as a control) or NNK-treated WT pseudo-A/J mice and *Adam17*$^{ex/ex}$ (ex/ex) pseudo-A/J mice (n = 5 to 8 per group). (*B*) Representative images of H&E-stained pancreatic sections from the indicated mice. Black arrowheads point to edematous areas, while green arrowheads point to immune cell infiltration. (Scale bars, 100 μm) (*C*) Histological disease severity scoring of pancreatic edema and inflammation in pancreatic tissues from the indicated groups (n = 5 to 8 per group). (*D*) Relative serum lipase activity in the indicated groups (n = 5 to 8 per group). (*E*, *G*, and *K*) Representative images of CD45-, pSer^{536} p65 NFκB-, and pTyr^{705} STAT3-stained pancreatic sections from the indicated mice, respectively. (Scale bars, 100 μm) (*F*, *H*, and *L*) Quantification of CD45-positive cells per HPF as well as pSer^{536} p65 NFκB- and pTyr^{705} STAT3-staining intensity in pancreatic tissues of the indicated groups (n = 5 per group), respectively. (*I*) qPCR expression analysis of *Il6* gene (normalized against *18s rRNA*) in pancreatic tissues from the indicated groups (n = 5 per group). (*J*) Serum levels of soluble IL-6R (sIL-6R; ng/mL) in the indicated groups (n = 5 per group). *P < 0.05, **P < 0.01, ***P < 0.001, ****P < 0.0001, one-way ANOVA.

pancreatic inflammation in the context of NNK-induced pancreatic injury.

Therapeutic Targeting of ADAM17 Ameliorates AP. We next sought to evaluate the anti-inflammatory effects of the recombinant ADAM17 prodomain inhibitor (A17pro) in both in vivo models of AP. Treatment of WT mice with a single IP injection of A17pro prior to the induction of cerulein-induced AP significantly reduced serum amylase levels, immune cell infiltrates (including T cells), acinar cell necrosis, and serum levels of sIL-6R, without affecting *Il6* levels (Fig. 6 *A–J*). Similarly, concomitant treatment of WT mice with NNK and A17pro suppressed NNK-induced pancreatic inflammation, indicated by decreased serum lipase levels, immune cell infiltration, and serum levels of sIL-6R, without affecting *Il6* levels (Fig. 6 *K–R*). These data reveal that the therapeutic blockade of ADAM17 cell surface activity using recombinant A17pro recapitulates the protective effects of the genetic deficiency of ADAM17 in *Adam17*$^{ex/ex}$ mice, which suggest that A17pro could be exploited as a therapeutic option in AP.

Deficiency of ADAM17 Protects against Chronic Pancreatic Fibrosis. CP is described as a fibroinflammatory syndrome of the exocrine pancreas (2). Therefore, we investigated the role of ADAM17 in promoting pancreatic stromal fibrosis and activation of myofibroblasts in a chronic model of NNK-induced pancreatitis. As shown in Fig. 7 *A–D*, reduced levels of Masson's trichome, which stains collagen fibers and indicates levels of stromal fibrotic depositions, and activated αSMA-positive myofibroblasts were observed in pancreatic tissues of NNK-challenged *Adam17*$^{ex/ex}$ mice compared to their WT controls. Consistent with data from AP models, ADAM17 deficiency also decreased serum levels of sIL-6R and STAT3 activation in pancreatic tissues (Fig. 7 *E–H*). Collectively, these data demonstrate that ADAM17 plays an important role in promoting pancreatic fibrosis in CP.

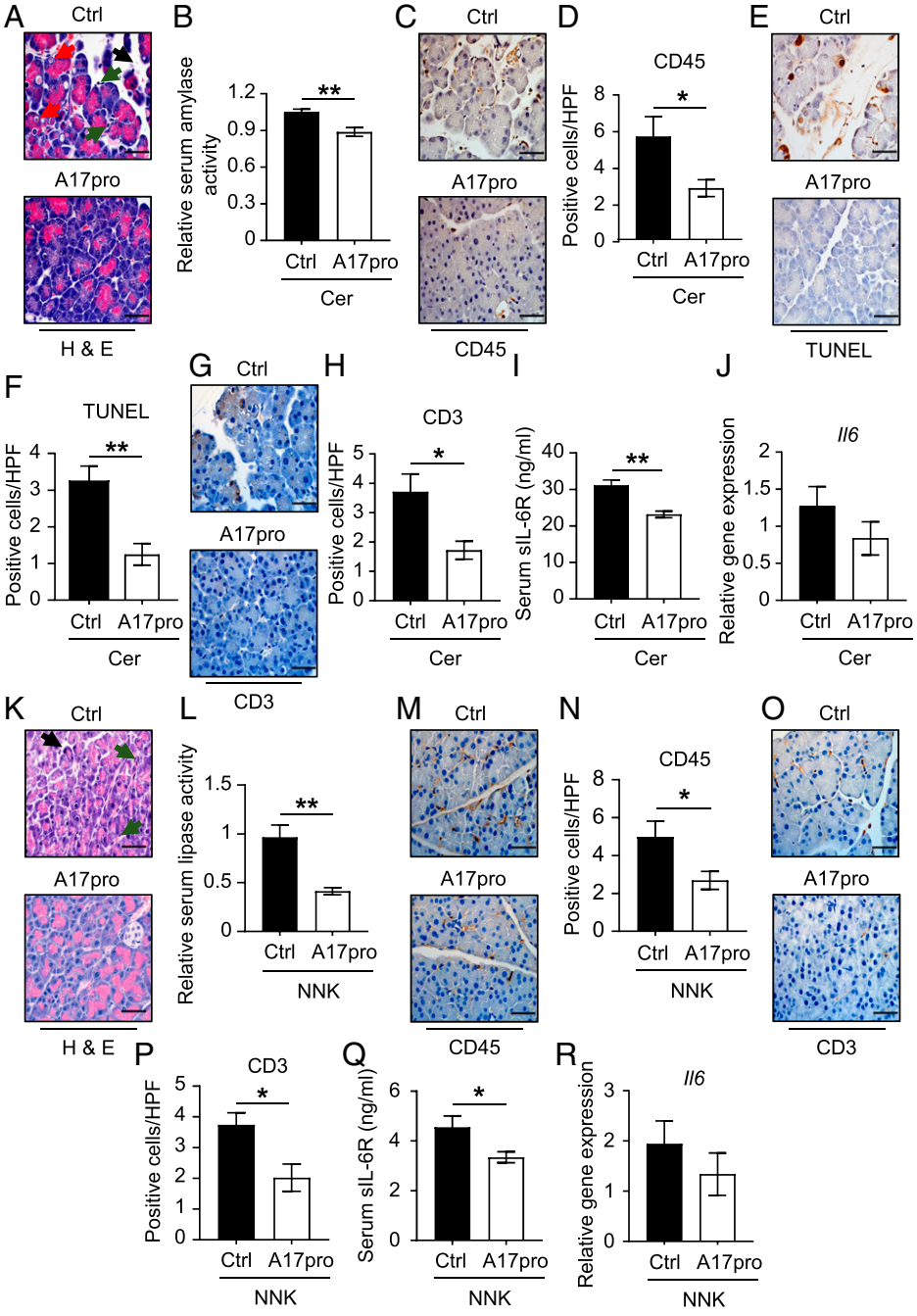

Fig. 6. Therapeutic blockade of ADAM17 cell surface activity using its recombinant prodomain (A17pro) alleviates experimental pancreatitis. (*A*) Representative images of H&E-stained pancreatic sections from WT mice treated with single IP injection of either PBS (as a control) or recombinant ADAM17 prodomain (A17pro) followed by cerulein-mediated pancreatitis induction. Black arrowheads point to edematous areas, green arrowheads point to immune cell infiltration, and red arrowheads point to necrotic cells. (Scale bars, 100 μm) (*B*) Relative serum amylase activity in the indicated groups (n = 6 to 8 per group). (*C*, *E*, and *G*) Representative images of CD45-, TUNEL-, and CD3-stained pancreatic sections from the indicated mice, respectively. (Scale bars, 100 μm) (*D*, *F*, and *H*) Quantification of CD45-, TUNEL-, and CD3-positive cells per HPF in pancreatic tissues of the indicated groups (n = 5 per group), respectively. (*I*) Serum levels of soluble IL-6R (sIL-6R; ng/mL) in the indicated groups (n = 6 to 8 per group). (*J*) qPCR expression analysis of *Il6* gene (normalized against *18s rRNA*) in pancreatic tissues from the indicated groups (n = 5 per group). (*K*) Representative images of H&E-stained pancreatic sections from WT pseudo-A/J mice treated with three IP injection of either PBS (as a control) or recombinant ADAM17 prodomain (1 mg/kg) concomitant with cigarette smoke carcinogen (NNK)-mediated pancreatitis induction. Black arrowheads point to edematous areas, while green arrowheads point to immune cell infiltration. (Scale bars, 100 μm) (*L*) Relative serum lipase activity in the indicated groups (n = 6 to 8 per group). (*M* and *O*) Representative images of CD45- and CD3-stained pancreatic sections from the indicated mice, respectively. (Scale bars, 100 μm) (*N* and *P*) Quantification of CD45- and CD3-positive cells per HPF in pancreatic tissues of the indicated groups (n = 5 per group), respectively. (*Q*) Serum levels of soluble IL-6R (sIL-6R; ng/mL) in the indicated groups (n = 6 to 8 per group). $^{*}P < 0.05$, $^{**}P < 0.01$, Student's t test. (*R*) qPCR expression analysis of *Il6* gene (normalized against *18s rRNA*) in pancreatic tissues from the indicated groups (n = 5 per group).

Up-Regulation of the ADAM17/IL-6 Trans-signaling/STAT3 Axis Is a Feature of Human Pancreatitis. The expression of ADAM17 in human pancreatitis is largely unknown. We therefore investigated ADAM17/IL-6 trans-signaling expression in patients with pancreatitis. IHC revealed that ADAM17 protein levels were up-regulated in acinar epithelial cells of pancreatitis patients compared to their normal controls (Fig. 8 *A* and *B*). Furthermore, serum levels of sIL-6R were also up-regulated in pancreatitis patients, and IHC indicated that enhanced STAT3 activity in pancreatic tissues positively correlated with ADAM17 protein expression levels (Fig. 8 *C*–*F*). Therefore, our clinical data are consistent with a key role for ADAM17 in promoting the pathogenesis of pancreatitis.

Discussion

Pancreatitis is a common and potentially life-threatening inflammatory disorder, yet its pathogenesis is not fully understood, and there are no effective targeted therapeutic approaches (42). Here we propose the ADAM17 protease as a highly promising therapeutic target in pancreatitis. Our clinical and preclinical data suggest that ADAM17 is markedly up-regulated in the pancreatic acinar epithelium during pancreatitis development. Moreover, genetic and therapeutic targeting of ADAM17 ameliorated pancreatic inflammation, apoptosis, and fibrosis in preclinical models of pancreatitis, which was accompanied by halting the overexpressed pathological IL-6 trans-signaling axis in pancreatic tissues. Importantly, inhibiting ADAM17 cell surface activity using the A17pro recombinant prodomain inhibitor recapitulated the protective effects of genetic deletion of ADAM17, suggesting that A17pro could represent a therapeutic option to target ADAM17 in the clinical setting of pancreatitis. We note that the *Adam17*$^{ex/ex}$ mouse strain used in our study displays a baseline phenotype that is restricted to eye, heart, and skin defects largely attributed to defective EGFR signaling (18). Therefore, we believe that baseline

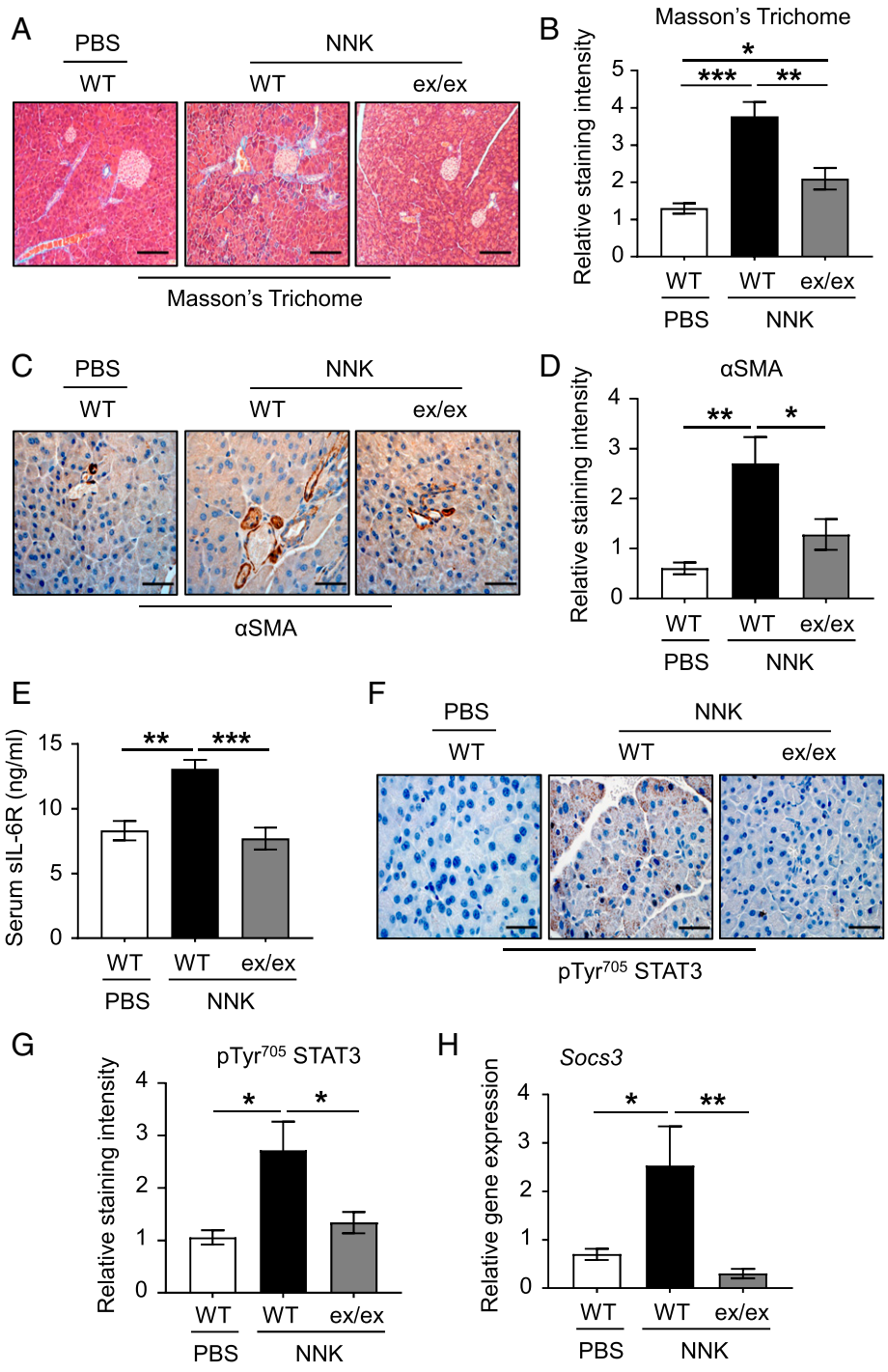

Fig. 7. Deficiency of ADAM17 halts the chronic fibrotic changes in pancreatic tissues subjected to the cigarette smoke carcinogen (NNK). (*A* and *C*) Representative images of Masson's trichome- and αSMA-stained pancreatic sections from PBS (as a control) or NNK-treated WT pseudo-A/J mice and *Adam17*$^{ex/ex}$ (ex/ex) pseudo-A/J mice treated with NNK, respectively. (Scale bars, 100 μm) (*B* and *D*) Quantification of Masson's trichome- and αSMA-staining intensity in pancreatic tissues of the indicated groups, respectively (n = 5 per group). (*E*) Serum levels of soluble IL-6R (sIL-6R; ng/mL) in the indicated groups (n = 5 per group). (*F*) Representative images of pTyr^{705} STAT3-stained pancreatic sections from the indicated groups. (Scale bars, 100 μm) (*G*) Quantification of pTyr^{705} STAT3-staining intensity in pancreatic tissues of the indicated groups (n = 5 per group). (*H*) qPCR expression analysis of *Socs3* gene (normalized against *18s rRNA*) in pancreatic tissues from the indicated groups (n = 5 per group). *P < 0.05, **P < 0.01, ***P < 0.001, one-way ANOVA.

alterations to the phenotype of *Adam17*$^{ex/ex}$ mice are independent of the pancreas and thus are unlikely to significantly impact our findings here related to pancreatitis.

Several immune cells have been described to infiltrate the pancreas following the onset of pancreatitis, which have been associated with disease severity and prognosis. These include innate immune cells such as macrophages, neutrophils, dendritic cells, and mast cells, as well as adaptive immune cells such as T and B lymphocytes (55). Indeed, T cells and neutrophils play an important role in fueling an inflammatory environment to promote pancreatitis (56). Also, ADAM17 shedding activity regulates neutrophil activation and extravasation as well as T cell activation and expansion (57, 58). Moreover, in acute inflammatory settings, IL-6 trans-signaling via sIL-6R induces T cell migration and neutrophil trafficking through activation of STAT3 (59, 60). Interestingly, a miniaturized chimeric soluble gp130 variant was recently reported to efficiently and specifically trap the IL-6/sIL-6R complex, resulting in inhibition of T cell expansion (61). In support of these observations, our in vivo findings suggest that ADAM17 increases biased T cell and neutrophil migration to the pancreas during pancreatitis, possibly via IL-6 trans-signaling. Notably, using reciprocal cerulein-stimulated acinar epithelial and T cell cultures from WT and *Adam17*$^{ex/ex}$ mice, we show that ADAM17-expressing epithelial cells can also augment IL-6 trans-signaling in vitro. Despite the predominant role of ADAM17 in epithelial versus T cell compartments in driving IL-6 trans-signaling in this in vitro setting of cerulein-induced pancreatitis, the involvement of ADAM17-expressing T cells (or other immune

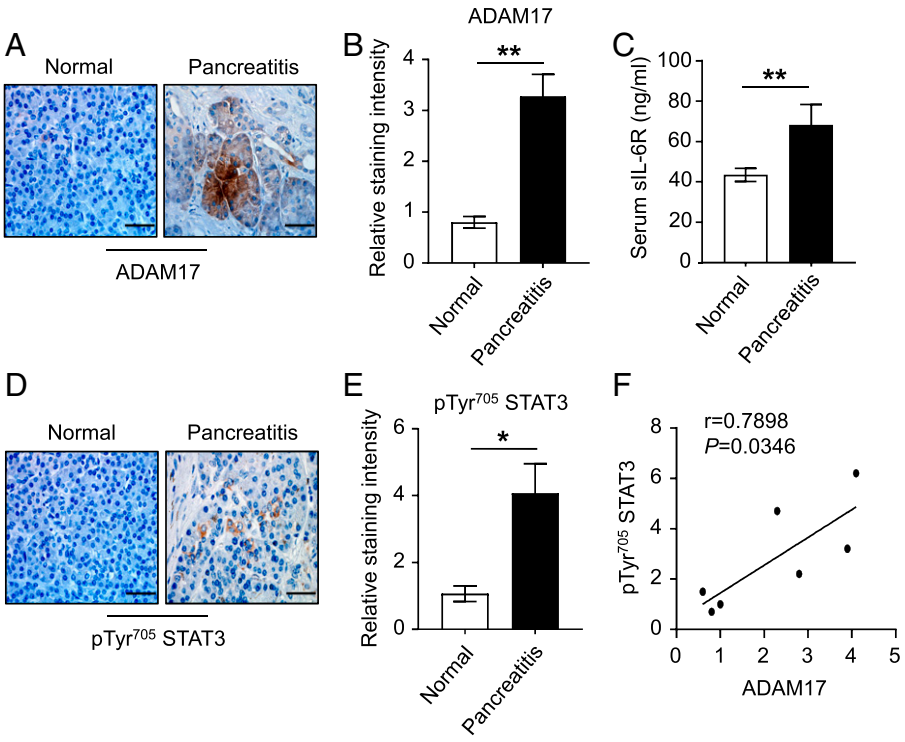

Fig. 8. Up-regulation of ADAM17/sIL-6R/pSTAT3 in human pancreatitis. (*A*) Representative images of ADAM17-stained pancreatic sections from non-cancerous normal and pancreatitis biopsies. (Scale bar, 100 μm) (*B*) Quantification of ADAM17 staining intensity in pancreatic tissues of the indicated groups (n = 3 to 4 per group). (*C*) Serum levels of soluble IL-6R (sIL-6R; ng/mL) in the indicated groups (n = 11 per group). (*D*) Representative images of pTyr^{705} STAT3-stained pancreatic sections from non-cancerous normal and pancreatitis biopsies. (Scale bar, 100 μm) (*E*) Quantification of pTyr^{705} STAT3 staining intensity in pancreatic tissues of the indicated groups (n = 3 to 4 per group). *P < 0.05, **P < 0.01, Student's t test. (*F*) Linear regression analysis of ADAM17 with pTyr^{705} STAT3 staining in pancreatic sections from non-cancerous normal and pancreatitis biopsies. r, Pearson correlation coefficient.

cell types) in ADAM17-mediated pancreatitis cannot be ruled out. Therefore, future work is warranted using conditional knock-out strains of ADAM17 to identify the cell type(s) of origin (i.e., epithelial, immune, and endothelial) in which ADAM17 drives pancreatitis.

Another key finding of this current study is that ADAM17 deficiency inhibits the up-regulated NF-κB and STAT3 signaling pathways in pancreatitis. NF-κB is activated rapidly upon induction of inflammation, resulting in up-regulation of inflammatory cytokines including TNFα, IL-6, and IL-1β, which have been associated with AP (43). Indeed, pharmacologic inhibition of NF-κB, albeit with non-specific inhibitors such as antioxidants, reduced the inflammatory response, necrosis, and other parameters of AP severity (45, 62). Similarly, several reports revealed that IL-6–dependent activation of STAT3 signaling in the pancreas is implicated in AP pathogenesis (14, 63). In this respect, pancreas-specific inactivation of STAT3 or SOCS3 implicated the IL-6 trans-signaling/STAT3 signaling cascade in the development of systemic complications during cerulein-induced AP (14). Specifically, STAT3 up-regulation in the pancreas increases the expression of the neutrophil attractant chemokine CXCL1, leading to pulmonary neutrophil accumulation and consequent acute lung injury (14). In this setting, the therapeutic targeting of the IL-6 trans-signaling/gp130/STAT3/CXCL1 signaling axis during pancreatitis attenuated the systemic complications of severe AP (14). Moreover, in a rat model of severe AP, administration of tocilizumab, a neutralizing antibody against IL-6, suppressed pancreas disease severity and associated lung injury, including serum amylase, C-reactive protein, lung surfactant protein level, and myeloperoxidase activity via inhibition of pancreatic NF-κB and STAT3 (64). However, the use of such therapeutic strategies, which do not discriminate between blocking "good" classical IL-6 signaling and "bad" pathological trans-signaling, is associated with severe adverse effects such as neutropenia and increased susceptibility to bacterial infections due to the blockade of homeostatic immune functions maintained by classical IL-6 signaling (16). On the other hand, blocking only the bad side of IL-6 signaling, either directly or via the ADAM17 protease, the latter as we show here in pancreatitis, offers an attractive therapeutic strategy for treating inflammatory diseases (65). Future studies are now warranted to assess the role of ADAM17 in severe AP complications including acute lung injury, which could be speculated from our recent discoveries of the proinflammatory role of ADAM17 in lung diseases and the wide distribution and colocalization of both ADAM17 and its preferred substrate IL-6R in the lung (11, 17, 19).

Finally, ADAM17 has been implicated in the development of various fibrotic disorders including kidney, lung, and vascular fibrosis (66–68). IL-6 trans-signaling is also shown to promote fibrotic changes in pulmonary, dermal, peritoneal, and renal tissues, possibly via activation of STAT3 pathway (69–72). Taken together, targeting ADAM17/IL-6 trans-signaling represents a promising option for clinical implication in a growing number of inflammatory conditions. In conclusion, our study defines the proinflammatory and profibrotic roles of the protease ADAM17 in pancreatitis and provides a rationale for strategies aimed at inhibiting ADAM17 activity to serve as therapeutic options for treating or preventing pancreatitis.

Data, Materials, and Software Availability. All study data are included in the article and/or *SI Appendix*.

ACKNOWLEDGMENTS. This work was supported by a research grant awarded by the National Health and Medical Research Council (NHMRC) of Australia to B.J.J., as well as the Operational Infrastructure Support Program by the Victorian Government of Australia. M.I.S. is supported by a Cancer Council Victoria Postdoctoral Fellowship. S.R.-J. was supported by the Deutsche Forschungsgemeinschaft, Bonn, Germany (CRC841, project C1, and CRC877, projects A1 and A14); by the Cluster of Excellence 306 "Precision Medicine in Chronic Inflammation"; and by the German Cancer Aid. B.J.J. is supported by an NHMRC Senior Medical Research Fellowship.

Author affiliations: [a]Department of Molecular and Translational Science, Faculty of Medicine, Nursing and Health Sciences, Monash University, Clayton, VIC 3800, Australia; [b]Centre for Innate Immunity and Infectious Diseases, Hudson Institute of Medical Research, Clayton, VIC 3168, Australia; [c]Department of Surgery, School of

Clinical Sciences, Monash University, VIC 3168, Australia; [d]Department of Anatomical Pathology, Monash Health, Clayton, VIC 3168, Australia; [e]Department of Biological Regulation, Weizmann Institute of Science, Rehovot 7610001, Israel; and [f]Institute of Biochemistry, Christian-Albrechts-University, Kiel 24118, Germany

Author contributions: M.I.S. and B.J.J. designed research; M.I.S., T.W., J.L., L.J.G., A.C.W., C.M.H., M.A., C.H., D.C., B.K., and B.J.J. performed research; D.C., I.S., and S.R.-J. contributed new reagents/analytic tools; M.I.S., T.W., J.L., L.J.G., B.K., and B.J.J. analyzed data; and M.I.S., S.R-J., and B.J.J. wrote the paper.

1. A. F. Peery *et al.*, Burden and cost of gastrointestinal, liver, and pancreatic diseases in the United States: Update 2018. Gastroenterology **156**, 254–272.e211 (2019).
2. G. Beyer, A. Habtezion, J. Werner, M. M. Lerch, J. Mayerle, Chronic pancreatitis. *Lancet* **396**, 499–512 (2020).
3. P. Sinonquel, W. Laleman, A. Wilmer, Advances in acute pancreatitis. *Curr. Opin. Crit. Care* **27**, 193–200 (2021).
4. D. C. Whitcomb, Clinical practice. Acute pancreatitis. *N. Engl. J. Med.* **354**, 2142–2150 (2006).
5. U. Ahmed Ali *et al.*; Dutch Pancreatitis Study Group, Risk of recurrent pancreatitis and progression to chronic pancreatitis after a first episode of acute pancreatitis. *Clin. Gastroenterol. Hepatol.* **14**, 738–746 (2016).
6. J. Mayerle *et al.*, Genetics, cell biology, and pathophysiology of pancreatitis. *Gastroenterology* **156**, 1951–1968.e1951 (2019).
7. S. Düsterhöft, J. Lokau, C. Garbers, The metalloprotease ADAM17 in inflammation and cancer. *Pathol. Res. Pract.* **215**, 152410 (2019).
8. M. I. Saad, S. Rose-John, B. J. Jenkins, ADAM17: An emerging therapeutic target for lung cancer. *Cancers (Basel)* **11**, 1218 (2019).
9. F. Zunke, S. Rose-John, The shedding protease ADAM17: Physiology and pathophysiology. *Biochim. Biophys. Acta Mol. Cell Res.* **1864**, 2059–2070 (2017).
10. E. Wong *et al.*, Harnessing the natural inhibitory domain to control TNFα converting enzyme (TACE) activity in vivo. *Sci. Rep.* **6**, 1–12 (2016).
11. M. I. Saad *et al.*, ADAM17 selectively activates the IL-6 trans-signaling/ERK MAPK axis in KRAS-addicted lung cancer. *EMBO Mol. Med.* **11**, e9976 (2019).
12. M. I. Saad *et al.*, The ADAM17 protease promotes tobacco smoke carcinogen-induced lung tumorigenesis. *Carcinogenesis* **41**, 527–538 (2020).
13. N. Schumacher, S. Rose-John, ADAM17 activity and IL-6 trans-signaling in inflammation and cancer. *Cancers (Basel)* **11**, 1736 (2019).
14. H. Zhang *et al.*, IL-6 trans-signaling promotes pancreatitis-associated lung injury and lethality. *J. Clin. Invest.* **123**, 1019–1031 (2013).
15. J. Scheller, C. Garbers, S. Rose-John, Interleukin-6: From basic biology to selective blockade of pro-inflammatory activities. *Semin. Immunol.* **26**, 2–12 (2014).
16. S. A. Jones, B. J. Jenkins, Recent insights into targeting the IL-6 cytokine family in inflammatory diseases and cancer. *Nat. Rev. Immunol.* **18**, 773–789 (2018).
17. R. E. Dawson, B. J. Jenkins, M. I. Saad, IL-6 family cytokines in respiratory health and disease. *Cytokine* **143**, 155520 (2021).
18. A. Chalaris *et al.*, Critical role of the disintegrin metalloprotease ADAM17 for intestinal inflammation and regeneration in mice. *J. Exp. Med.* **207**, 1617–1624 (2010).
19. M. I. Saad *et al.*, ADAM17 deficiency protects against pulmonary emphysema. *Am. J. Respir. Cell Mol. Biol.* **64**, 183–195 (2021).
20. A. Miller, G. D. Brooks, L. McLeod, S. Ruwanpura, B. J. Jenkins, Differential involvement of gp130 signalling pathways in modulating tobacco carcinogen-induced lung tumourigenesis. *Oncogene* **34**, 1510–1519 (2015).
21. J. Gout *et al.*, Isolation and culture of mouse primary pancreatic acinar cells. *J. Vis. Exp.* **78**, 50514 (2013).
22. R Core Team, *R: A Language and Environment for Statistical Computing* (R Foundation for Statistical Computing, Vienna, Austria, 2013). www.R-project.org/.
23. L. Tian *et al.*, scPipe: A flexible R/Bioconductor preprocessing pipeline for single-cell RNA-sequencing data. *PLOS Comput. Biol.* **14**, e1006361 (2018).
24. Y. Liao, G. K. Smyth, W. Shi, The R package Rsubread is easier, faster, cheaper and better for alignment and quantification of RNA sequencing reads. *Nucleic Acids Res.* **47**, e47 (2019).
25. S. Durinck, P. T. Spellman, E. Birney, W. Huber, Mapping identifiers for the integration of genomic datasets with the R/Bioconductor package biomaRt. *Nat. Protoc.* **4**, 1184–1191 (2009).
26. M. D. Robinson, D. J. McCarthy, G. K. Smyth, edgeR: A Bioconductor package for differential expression analysis of digital gene expression data. *Bioinformatics* **26**, 139–140 (2010).
27. M. D. Robinson, A. Oshlack, A scaling normalization method for differential expression analysis of RNA-seq data. *Genome Biol.* **11**, R25 (2010).
28. C. W. Law, Y. Chen, W. Shi, G. K. Smyth, voom: Precision weights unlock linear model analysis tools for RNA-seq read counts. *Genome Biol.* **15**, R29 (2014).
29. M. E. Ritchie *et al.*, limma powers differential expression analyses for RNA-sequencing and microarray studies. *Nucleic Acids Res.* **43**, e47 (2015).
30. D. J. McCarthy, G. K. Smyth, Testing significance relative to a fold-change threshold is a TREAT. *Bioinformatics* **25**, 765–771 (2009).
31. R. Kolde, pheatmap: Pretty Heatmaps. R package version 1.0. 12. CRAN.R-project.org/package=pheatmap (2019).
32. A. Subramanian *et al.*, Gene set enrichment analysis: A knowledge-based approach for interpreting genome-wide expression profiles. *Proc. Natl. Acad. Sci. U.S.A.* **102**, 15545–15550 (2005).
33. I. Dolgalev, MSigDB Gene Sets for Multiple Organisms in a Tidy Data Format [R package msigdbr version 7.0. 1]. Comprehensive R Archive Network (CRAN), https://CRAN.R-project.org/package (2020).
34. D. Wu, G. K. Smyth, Camera: A competitive gene set test accounting for inter-gene correlation. *Nucleic Acids Res.* **40**, e133–e133 (2012).
35. B. Phipson, S. Lee, I. J. Majewski, W. S. Alexander, G. K. Smyth, Robust hyperparameter estimation protects against hypervariable genes and improves power to detect differential expression. *Ann. Appl. Stat.* **10**, 946–963 (2016).
36. A. Asayesh, T. Alanentalo, N. K. Khoo, U. Ahlgren, Developmental expression of metalloproteases ADAM 9, 10, and 17 becomes restricted to divergent pancreatic compartments. *Dev. Dyn.* **232**, 1105–1114 (2005).
37. P. S. Leung, S. P. Ip, Pancreatic acinar cell: Its role in acute pancreatitis. *Int. J. Biochem. Cell Biol.* **38**, 1024–1030 (2006).
38. L. Jin, S. Batra, D. N. Douda, N. Palaniyar, S. Jeyaseelan, CXCL1 contributes to host defense in polymicrobial sepsis via modulating T cell and neutrophil functions. *J. Immunol.* **193**, 3549–3558 (2014).
39. D. Awla *et al.*, NFATc3 regulates trypsinogen activation, neutrophil recruitment, and tissue damage in acute pancreatitis in mice. *Gastroenterology* **143**, 1352–1360.e1357 (2012).
40. M. Gershkovitz, T. Fainsod-Levi, T. Zelter, R. V. Sionov, Z. Granot, TRPM2 modulates neutrophil attraction to murine tumor cells by regulating CXCL2 expression. *Cancer Immunol. Immunother.* **68**, 33–43 (2019).
41. K. Saeki *et al.*, CCL2-induced migration and SOCS3-mediated activation of macrophages are involved in cerulein-induced pancreatitis in mice. *Gastroenterology* **142**, 1010–1020.e1019 (2012).
42. P. J. Lee, G. I. Papachristou, New insights into acute pancreatitis. *Nat. Rev. Gastroenterol. Hepatol.* **16**, 479–496 (2019).
43. Z. Rakonczay, Jr, P. Hegyi, T. Takács, J. McCarroll, A. K. Saluja, The role of NF-kappaB activation in the pathogenesis of acute pancreatitis. *Gut* **57**, 259–267 (2008).
44. A. P. Clemons, D. M. Holstein, A. Galli, C. Saunders, Cerulein-induced acute pancreatitis in the rat is significantly ameliorated by treatment with MEK1/2 inhibitors U0126 and PD98059. *Pancreas* **25**, 251–259 (2002).
45. T.-H. Kim *et al.*, 2′,4′,6′-Tris(methoxymethoxy) chalcone (TMMC) attenuates the severity of cerulein-induced acute pancreatitis and associated lung injury. *Am. J. Physiol. Gastrointest. Liver Physiol.* **301**, G694–G706 (2011).
46. A. C. Wagner, W. Metzler, T. Höfken, H. Weber, B. Göke, p38 map kinase is expressed in the pancreas and is immediately activated following cerulein hyperstimulation. *Digestion* **60**, 41–47 (1999).
47. M.-H. Cao *et al.*, p38 MAPK inhibition alleviates experimental acute pancreatitis in mice. *Hepatobiliary Pancreat. Dis. Int.* **14**, 101–106 (2015).
48. L. Pistoni *et al.*; PanGenEU Study Investigators, Associations between pancreatic expression quantitative traits and risk of pancreatic ductal adenocarcinoma. *Carcinogenesis* **42**, 1037–1045 (2021).
49. W. Li *et al.*, Identification and prognostic analysis of biomarkers to predict the progression of pancreatic cancer patients. *Mol. Med.* **28**, 43 (2022).
50. J. Hillion *et al.*, The HMGA1-COX-2 axis: A key molecular pathway and potential target in pancreatic adenocarcinoma. *Pancreatology* **12**, 372–379 (2012).
51. M. Treiber *et al.*, Keratin 8 sequence variants in patients with pancreatitis and pancreatic cancer. *J. Mol. Med. (Berl.)* **84**, 1015–1022 (2006).
52. N. Jia *et al.*, CLIC1 overexpression is associated with poor prognosis in pancreatic ductal adenocarcinomas. *J. Cancer Res. Ther.* **12**, 892–896 (2016).
53. A. A. Alahmari *et al.*, Cigarette toxin 4-(methylnitrosamino)-1-(3-pyridyl)-1-butanone (NNK) induces experimental pancreatitis through α7 nicotinic acetylcholine receptors (nAChRs) in mice. *PLoS One* **13**, e0197362 (2018).
54. O. Z. Ismail, V. Bhayana, Lipase or amylase for the diagnosis of acute pancreatitis? *Clin. Biochem.* **50**, 1275–1280 (2017).
55. C. Peng, Z. Li, X. Yu, The role of pancreatic infiltrating innate immune cells in acute pancreatitis. *Int. J. Med. Sci.* **18**, 534–545 (2021).
56. J. Xue, V. Sharma, A. Habtezion, Immune cells and immune-based therapy in pancreatitis. *Immunol. Res.* **58**, 378–386 (2014).
57. U. Schaff, P. E. Mattila, S. I. Simon, B. Walcheck, Neutrophil adhesion to E-selectin under shear promotes the redistribution and co-clustering of ADAM17 and its proteolytic substrate L-selectin. *J. Leukoc. Biol.* **83**, 99–105 (2008).
58. R. N. Mohammed *et al.*, ADAM17-dependent proteolysis of L-selectin promotes early clonal expansion of cytotoxic T cells. *Sci. Rep.* **9**, 5487 (2019).
59. R. M. McLoughlin *et al.*, IL-6 trans-signaling via STAT3 directs T cell infiltration in acute inflammation. *Proc. Natl. Acad. Sci. U.S.A.* **102**, 9589–9594 (2005).
60. C. A. Fielding *et al.*, IL-6 regulates neutrophil trafficking during acute inflammation via STAT3. *J. Immunol.* **181**, 2189–2195 (2008).
61. D. Heise *et al.*, Selective inhibition of IL-6 trans-signaling by a miniaturized, optimized chimeric soluble gp130 inhibits T_H17 cell expansion. *Sci. Signal.* **14**, eabc3480 (2021).
62. M. A. Kanak *et al.*, A small molecule inhibitor of NFκB blocks ER stress and the NLRP3 inflammasome and prevents progression of pancreatitis. *J. Gastroenterol.* **52**, 352–365 (2017).
63. J. H. Yu, K. H. Kim, H. Kim, SOCS 3 and PPAR-γ ligands inhibit the expression of IL-6 and TGF-β1 by regulating JAK2/STAT3 signaling in pancreas. *Int. J. Biochem. Cell Biol.* **40**, 677–688 (2008).
64. K.-L. Chen *et al.*, Effects of tocilizumab on experimental severe acute pancreatitis and associated acute lung injury. *Crit. Care Med.* **44**, e664–e677 (2016).
65. S. Rose-John, Blocking only the bad side of IL-6 in inflammation and cancer. *Cytokine* **148**, 155690 (2021).
66. E. Kefaloyianni *et al.*, ADAM17 substrate release in proximal tubule drives kidney fibrosis. *JCI Insight* **1**, 87023 (2016).
67. T. Takayanagi *et al.*, Vascular ADAM17 as a novel therapeutic target in mediating cardiovascular hypertrophy and perivascular fibrosis induced by angiotensin II. *Hypertension* **68**, 949–955 (2016).
68. J. Ge *et al.*, Association of ADAM17 expression levels in patients with interstitial lung disease. *Immunol. Invest.* **49**, 134–145 (2020).
69. T.-T. T. Le *et al.*, Blockade of IL-6 Trans signaling attenuates pulmonary fibrosis. *J. Immunol.* **193**, 3755–3768 (2014).
70. S. O'Reilly, M. Ciechomska, R. Cant, J. M. van Laar, Interleukin-6 (IL-6) trans signaling drives a STAT3-dependent pathway that leads to hyperactive transforming growth factor-β (TGF-β) signaling promoting SMAD3 activation and fibrosis via Gremlin protein. *J. Biol. Chem.* **289**, 9952–9960 (2014).
71. W. Chen *et al.*, Blocking interleukin-6 trans-signaling protects against renal fibrosis by suppressing STAT3 activation. *Theranostics* **9**, 3980–3991 (2019).
72. X. Yang *et al.*, IL-6 *trans*-signaling drives a STAT3-dependent pathway that leads to structural alterations of the peritoneal membrane. *Am. J. Physiol. Renal Physiol.* **318**, F338–F353 (2020).